Lorentz violation effects in $2\nu\beta\beta$ decay

O Niţescu[1,2,3,4] ⓘ, S Ghinescu[1,2,3,4] ⓘ and S Stoica[1,2] ⓘ

[1] International Centre for Advanced Training and Research in Physics, PO Box MG12, 077125-Magurele, Romania
[2] Horia Hulubei National Institute of Physics and Nuclear Engineering, PO Box MG6, 077125-Magurele, Romania
[3] University of Bucharest, Faculty of Physics, PO Box MG11, 077125-Magurele, Romania

E-mail: sabin.stoica@cifra.infim.ro

CrossMark

Abstract

Observable effects for the Lorentz invariance violation (LIV) at a low energy scale can also be investigated in double beta decay. For example, by comparing the theoretical predictions with a precise analysis of the summed energy spectra of electrons in $2\nu\beta\beta$ decay, one can constrain the $\mathring{a}_{\text{of}}^{(3)}$ coefficient that governs the time-like component of the Lorentz invariance violating operator that appears in the Standard Model extension theory. In this work, we perform calculations of the phase space factors (PSF) and summed energy spectra of electrons as well as of their deviations due to LIV necessary in such experimental investigations. The Fermi functions needed in the calculation are built up with exact electron wave functions obtained by numerically solving the Dirac equation in a realistic Coulomb-type potential with the inclusion of the finite nuclear size and screening effects. We compared our results with those used in previous LIV investigations that were obtained with approximate (analytical) Fermi functions and found differences of up to 30% for heavier nuclei. Our work includes eight experimentally interesting nuclei. Next, we estimate and discuss the uncertainties of our calculations associated with uncertainties in Q-values measurements and the differences raised from the inclusion of the kinematic terms in the formalism. Finally, we provide the ratio between the standard PSF and their LIV deviations and the energies where the LIV effects are expected to be maximal. We expect our study to be useful in the current LIV investigations in $2\nu\beta\beta$ decay and to lead to improved constraints on the $\mathring{a}_{\text{of}}^{(3)}$ coefficient.

Keywords: Lorentz invariance violation, double beta decay, phase space factors, electron spectra

[4] Authors contributed equally to this work.

(Some figures may appear in colour only in the online journal)

1. Introduction

There is a currently increasing interest in testing possible violations of fundamental symmetries in physical processes, one of them being the Lorentz invariance. The general theory that incorporates LIV is the Standard-Model extension (SME), which was developed by including Lorentz-violating terms in the Lagrange density [1–4]. These terms are constructed as coordinate-invariant products of a Lorentz invariance violating operator and a coefficient that controls the LIV size. The LIV operators can be of arbitrarily large dimension. Still, a particular interest represents the minimal SME, a limiting case of the SME theory that includes only LIV operators of mass dimension four or less [4]. Direct observation of LIV implies the investigation of physics at the Plank scale, which is not possible at the moment. However, it may be possible that LIV effects can manifest at a low energy scale and be potentially observable with current or near-future experimental techniques. For example, the experiments dedicated to the investigation of neutrino properties can be a framework where visible effects of LIV can be searched. The operators that couple to neutrinos in SME affect neutrino oscillations, neutrinos velocity and the electron spectra in beta and double-beta decays [5–9]. Effects of LIV have been searched in many neutrino oscillation experiments as Double-Chooz [10], MiniBooNE [11], IceCube [12], MINOS [13], SuperKamiokande [14] which obtained constraints on the corresponding coefficients. However, LIV in the neutrino sector can also be induced by a Lorentz-violating operator in SME, called countershaded operator, which does not affect the neutrino oscillations and which also breaks the CPT symmetry. The LIV effects related to this operator are controlled by the oscillation-free (of) coefficient with four components, one time-like $(a_{of}^{(3)})_{00}$ and three space-like $(a_{of}^{(3)})_{1m}$, with $m = 0, \pm 1$ [5]. Non-zero values of $(a_{of}^{(3)})_{00}$ coefficient would produce small deviations in the shape of the energy spectra of electrons emitted in beta and double-beta decays [9]. Such investigations were recently performed in the double beta decay (DBD) collaborations EXO [15], GERDA [16], SuperNEMO [17], CUORE [18, 19] and CUPID-0[20], and the non-observation of LIV effects resulted in constrains of the isotropic coefficient $\mathring{a}_{of}^{(3)} = (a_{of}^{(3)})_{00}/\sqrt{4\pi}$ [7]. However, in most of these analyses, the necessary theoretical ingredients were calculated with approximate (analytical) Fermi functions [21–24].

In this paper, we perform calculations of the phase space factors (PSF), summed energy spectra of electrons and their deviations necessary in LIV investigations from DBD experiments. The Fermi functions needed in the calculation are built with exact electron wave functions obtained by numerically solving a Dirac equation in a realistic Coulomb-type potential, with the inclusion of finite nuclear size and screening effects using a method described in our previous papers [25, 26]. We compared our results with those used in previous LIV investigations, which were obtained with approximate (analytical) Fermi functions, and found differences up to 30% for heavier nuclei. Our study includes the nuclei ^{48}Ca, ^{76}Ge, ^{82}Se, ^{100}Mo, ^{110}Pd, ^{116}Cd, ^{130}Te and ^{136}Xe. Next, we estimate and discuss the uncertainties in our calculations associated with uncertainties in Q-values measurements and the differences raised from the inclusion of the kinematic terms in the formalism. The Q-values and their uncertainties were obtained for each nucleus by averaging values reported in the literature by using a statistical procedure recommended by the Particle Data Group [27]. Finally, we provide for each nucleus the ratio between the standard PSF and their LIV deviations and the energies where the LIV effects are expected to be maximal. We expect our

study to be useful in the current LIV investigations in $2\nu\beta\beta$ decays and to lead to improved constraints on the $\mathring{a}_{\text{of}}^{(3)}$ coefficient.

2. Formalism

The interactions of neutrinos with the countershaded operator modify their four-component momentum from the standard expression $q^{\alpha} = (\omega, \mathbf{q})$ to $q^{\alpha} = (\omega, \mathbf{q} + \mathbf{a}_{\text{of}}^{(3)} - \mathring{a}_{\text{of}}^{(3)} \hat{\mathbf{q}})$ [4, 9, 28]. Considering this modification, the $2\nu\beta\beta$ decay rate can be written as a sum of two components:

$$\Gamma = \Gamma_0 + \delta\Gamma, \tag{1}$$

where Γ_0 is the standard decay rate and $\delta\Gamma$ is the perturbation induced by LIV. As known, the standard $2\nu\beta\beta$ decay rate can be written in a good approximation as follows [29]:

$$\Gamma_0 = g_A^4 |m_e c^2 M^{2\nu}|^2 G^{2\nu}. \tag{2}$$

In this expression g_A is the axial vector constant, $M^{2\nu}$ (in MeV^{-1}) is the nuclear matrix element and $G^{2\nu}$ is the PSF of the transition. Lorentz-violating effects in DBD appear as kinematical effects modifying only the PSF. Thus, the decay rate induced by LIV can be written in the form:

$$\delta\Gamma = g_A^4 |m_e c^2 M^{2\nu}|^2 \delta G^{2\nu}, \tag{3}$$

where $\delta G^{2\nu}$ is the PSF perturbation due to LIV. In what follows, we adopt the natural units ($\hbar = c = 1$), and we write the energy variables in units of m_e. For a $2\nu\beta\beta$ transition to the ground state (g.s.) of the daughter nucleus, the PSF expression reads:

$$\begin{aligned}
G^{2\nu} = C_1 \int_0^Q \mathrm{d}\epsilon_1 \int_0^{Q-\epsilon_1} \mathrm{d}\epsilon_2 \int_0^{Q-\epsilon_1-\epsilon_2} \mathrm{d}\omega_1 \\
\times F(Z_f, \epsilon_1) F(Z_f, \epsilon_2) \sqrt{\epsilon_1(\epsilon_1+2)}(\epsilon_1+1) \sqrt{\epsilon_2(\epsilon_2+2)}(\epsilon_2+1) \\
\times \omega_1^2 (Q - \epsilon_1 - \epsilon_2 - \omega_1)^2 (\langle K_N \rangle^2 + \langle L_N \rangle^2 + \langle K_N \rangle \langle L_N \rangle),
\end{aligned} \tag{4}$$

where $C_1 = (\tilde{A}^2 G_F^4 |V_{ud}|^4 m_e^9)/(96\pi^7 \ln 2)$, G_{F} is the Fermi coupling constant and V_{ud} the first element of the CKM matrix. $\epsilon_{1,2}$ and ω_1 are the energies of the electrons and of one antineutrino emitted in the decay and $F(Z, \epsilon)$ is the Fermi function. $\langle K_N \rangle$, $\langle L_N \rangle$ are kinematic factors that depend on the electrons and antineutrinos energies, on the g.s. energy E_I of the parent nucleus and on an averaged energy $\langle E_N \rangle$ of the excited states in the intermediate nucleus (closure approximation) [22]

$$\langle K_N \rangle = \frac{1}{\epsilon_1 + \omega_1 + \langle E_N \rangle - E_I + 1} + \frac{1}{\epsilon_2 + \omega_2 + \langle E_N \rangle - E_I + 1}, \tag{5}$$

$$\langle L_N \rangle = \frac{1}{\epsilon_1 + \omega_2 + \langle E_N \rangle - E_I + 1} + \frac{1}{\epsilon_2 + \omega_1 + \langle E_N \rangle - E_I + 1}. \tag{6}$$

Here, the difference in energy in the denominator can be obtained from the approximation $\tilde{A}^2 = [Q/2 + \langle E_N \rangle - E_I + 1]^2$, where $\tilde{A} = 1.12 A^{1/2}$ (in MeV) gives the energy of the giant Gamow–Teller resonance in the intermediate nucleus.

In order to evaluate $\delta G^{2\nu}$ from equation (4), we make use of the differential element of the antineutrino momentum which, from $\mathrm{d}^3 q = 4\pi \omega^2 \mathrm{d}\omega$ in the standard case, now becomes $\mathrm{d}^3 q = 4\pi (\omega^2 + 2\mathring{a}_{\text{of}}^{(3)} \omega) \mathrm{d}\omega$. Thus LIV contribution reads:

$$\delta G^{2\nu} = 10 \mathring{a}_{\text{of}}^{(3)} C_2 \int_0^Q d\epsilon_1 \int_0^{Q-\epsilon_1} d\epsilon_2 \int_0^{Q-\epsilon_1-\epsilon_2} d\omega_1$$
$$\times F(Z_f, \epsilon_1) F(Z_f, \epsilon_2) \sqrt{\epsilon_1(\epsilon_1 + 2)}(\epsilon_1 + 1) \sqrt{\epsilon_2(\epsilon_2 + 2)}(\epsilon_2 + 1)$$
$$\times \omega_1 (Q - \epsilon_1 - \epsilon_2 - \omega_1)^2 (\langle K_N \rangle^2 + \langle L_N \rangle^2 + \langle K_N \rangle \langle L_N \rangle), \tag{7}$$

where $C_2 = (\tilde{A}^2 G_F^4 |V_{ud}|^4 m_e^8)/(240\pi^7 \ln 2)$. The isotropic coefficient $\mathring{a}_{\text{of}}^{(3)}$, which governs the Lorentz violation strength, is the quantity of interest.

We note here that by making the approximation:

$$\langle K_N \rangle \simeq \langle L_N \rangle \simeq \frac{2}{E_I - \langle E_N \rangle - (Q/2 + 1)} \tag{8}$$

together with the approximation on $\tilde{A}$ and integrating over the energy of the antineutrino ω_1, one retrieves simplified expressions for the PSF which were used in many previous DBD works (see for example [24] and references therein) and also in the previous LIV analyzes [15, 17, 20]:

$$G^{2\nu} = C_3 \int_0^Q d\epsilon_1 \int_0^{Q-\epsilon_1} d\epsilon_2 F(Z_f, \epsilon_1) F(Z_f, \epsilon_2)$$
$$\times \sqrt{\epsilon_1(\epsilon_1 + 2)}(\epsilon_1 + 1) \sqrt{\epsilon_2(\epsilon_2 + 2)}(\epsilon_2 + 1)(Q - \epsilon_1 - \epsilon_2)^5, \tag{9}$$

$$\delta G^{2\nu} = 10 \mathring{a}_{\text{of}}^{(3)} C_4 \int_0^Q d\epsilon_1 \int_0^{Q-\epsilon_1} d\epsilon_2 F(Z_f, \epsilon_1) F(Z_f, \epsilon_2)$$
$$\times \sqrt{\epsilon_1(\epsilon_1 + 2)}(\epsilon_1 + 1) \sqrt{\epsilon_2(\epsilon_2 + 2)}(\epsilon_2 + 1)(Q - \epsilon_1 - \epsilon_2)^4, \tag{10}$$

where $C_3 = (G_F^4 |V_{ud}|^4 m_e^9)/(240\pi^7 \ln 2)$ and $C_4 = (G_F^4 |V_{ud}|^4 m_e^8)/(240\pi^7 \ln 2)$.

As seen from the above expressions, the main ingredients in the PSF calculation are the Fermi functions, which encodes the distortion of the electron wave functions due to the Coulomb field of the daughter nucleus, the kinematic factors $\langle K_N \rangle$, $\langle L_N \rangle$ and the Q-values. In the next sections, we refer to their use in the computation of the quantities relevant for analyzing of LIV effects in $2\nu\beta\beta$ decay.

3. Fermi functions

In this section, different approximation schemes used for the calculation of the Fermi function are briefly presented.

3.1. The approximation scheme A

In an early derivation of the $2\nu\beta\beta$ decay rate Primakoff and Rosen [21] and Konopinski [30], considered a non-relativistic movement of the emitted electrons in a Coulomb potential given by a point-like nucleus. The correction to the electron wave function can be derived by taking the square of the ratio between the Schrödinger scattering solution for a point charge Z_f and a plane wave, evaluated at the origin. In this case

$$F(Z_f, \epsilon) = F^{NR}(Z_f, \epsilon) = \frac{2\pi\eta}{1 - e^{-2\pi\eta}}, \tag{11}$$

where $\eta = \pm \alpha Z_f \epsilon / p$ ('+' corresponds to electrons and '−' to positrons), $\alpha \simeq 1/137$ is the fine structure constant, ϵ is the energy of the outgoing particle and $p = |\vec{p}|$ is their momentum.

Although this approximation fails badly for heavy nuclei (for example, a factor of 5 enhancement of the ^{130}Te PSF [31]), its use has the advantage that DBD rate can be integrated analytically and the obtained expression of the decay rate is a polynomial in powers of the Q-value.

3.2. The approximation scheme B

Adopting a relativistic treatment, the Fermi function is obtained as solution of a Dirac equation in a Coulomb potential given by a point charge (the finite size of the nucleus is neglected). It can still be expressed in an analytical form as:

$$F(Z_f, \epsilon) = F_0(Z_f, \epsilon) = 4(2pR_A)^{2(\gamma-1)}e^{\pi\eta}\frac{|\Gamma(\gamma + i\eta)|^2}{[\Gamma(2\gamma + 1)]^2}, \qquad (12)$$

with

$$\gamma = \sqrt{1 - (\alpha Z_f)^2}, \qquad \eta = \pm\alpha Z_f \epsilon / p \qquad (13)$$

with the same sign convention as above. R_A is the cut-off radius in the evaluation of the Dirac equation which is taken to match the radius of the daughter nucleus (i.e. $R_A = 1.2A^{1/3}$ fm). This approximation scheme was used extensively in the past [22–24] and will also be used here for comparison. We also note that in those works, the Gamma functions were computed using approximate expressions. In our case, the above expression of the Fermi function was computed using an exact form of the Gamma function and the results agree (within a few percentages) with the ones from [22–24].

3.3. The approximation scheme C

The Fermi function is built up from the radial solutions of the Dirac equation:

$$F(Z_f, \epsilon) = \frac{f_1^2(\epsilon, R_A) + g_{-1}^2(\epsilon, R_A)}{2p^2}, \qquad (14)$$

where f_1 and g_{-1} are the radial wave functions of the electron in the $s_{1/2}$ state evaluated at the nuclear radius $R_A = 1.2A^{1/3}$, which satisfy the radial Dirac equations [32]

$$\left(\frac{d}{dr} + \frac{\kappa + 1}{r}\right)g_\kappa(\epsilon, r) = (\epsilon - V(r) + 1)f_\kappa(\epsilon, r)$$
$$\left(\frac{d}{dr} - \frac{\kappa - 1}{r}\right)f_\kappa(\epsilon, r) = -(\epsilon - V(r) - 1)g_\kappa(\epsilon, r). \qquad (15)$$

The relativistic quantum number κ, takes positive and negative integer values. Total angular momentum of the electron is given by $j_\kappa = |\kappa| - 1/2$. The input central potential $V(r)$ includes the finite nuclear size correction and is built from a realistic proton charge density of the daughter nucleus:

$$\rho_e(\vec{r}) = \sum_i (2j_i + 1)v_i^2 |\psi_i(\vec{r})|^2, \qquad (16)$$

where j_i is the proton spin, v_i is the occupation amplitude of the proton wave function ψ_i of the spherical single particle state i, numerically determined as solution of the Schrödinger equation with a Wood–Saxon potential. The daughter nucleus potential is given by

$$V(Z, r) = \alpha \hbar c \int \frac{\rho_e(\vec{r'})}{|\vec{r} - \vec{r'}|} \mathrm{d}\vec{r'}. \tag{17}$$

This form of the potential includes diffuse nuclear surface corrections. Further, the screening effect of atomic electrons is taken into account following a prescription described in [33], by multiplying the expression of $V(r)$ with a function $\phi(r)$, which is solution of the Thomas–Fermi equation

$$\frac{\mathrm{d}^2\phi}{\mathrm{d}x^2} = \frac{\phi^{3/2}}{\sqrt{x}}, \tag{18}$$

with $x = r/b$, $b \approx 0.8853 a_0 Z^{-1/3}$ and a_0 is the Bohr radius. The method used to solve numerically the Thomas–Fermi equation is the Majorana method [34]. The solutions of the Dirac equation were obtained using our code that was built up following the numerical procedure presented in the [35–37]. This treatment of computing the Fermi function was also used by different authors [33, 38, 39], but the use of a realistic Coulomb potential was introduced only in [25, 26].

4. Comparison between Fermi functions

In earlier PSF calculations using approximate (analytical) forms of Fermi functions, the finite nuclear size or screening effects were not considered in computations, which can have a notable impact on the accuracy of the $2\nu\beta\beta$ decay related predictions, required in precise measurements. In this section, we calculate the PSF values and their deviations, using the equations (9) and (10) (without the inclusion of kinematic factors, as they were used in previous LIV analyzes). For the LIV perturbation, relevant is the quantity $\delta G^{2\nu}/(10\mathring{a}_{\mathrm{of}}^{(3)})$, which is independent on the LIV coefficient and is used by the experimentalists to constrain it.

The results are shown in table 1 wherein the upper part are displayed the PSF values, while in the lower part their deviations. Computations are done for the eight nuclei shown in the first column. The second column indicates the Q-values for each decay (obtained with the recipe described in the appendix), while in the next three columns are presented the $G^{2\nu}$ and $\delta G^{2\nu}/(10\mathring{a}_{\mathrm{of}}^{(3)})$ values with Fermi functions obtained in the approximation schemes A, B, and C. As expected, there are significant differences between the non-relativistic approximation A and the relativistic ones B, C. The non-relativistic treatment underestimates much the PSF values. However, there are also relevant differences between the PSF values calculated with Fermi functions obtained with treatments B and C. The approximation scheme B overestimates the PSF values as compared with C, and the differences between the two sets of values increase with the nuclear mass from about 8% for ^{48}Ca to about 30% for ^{136}Xe. Thus, the non-relativistic treatment of the Fermi functions is inadequate for LIV analyzes. In contrast, the use of exact radial solutions of the Dirac equation for building Fermi functions brings relevant corrections to the $G^{2\nu}$ and $\delta G^{2\nu}$ values as compared with those obtained with analytical expressions.

5. Electron spectra

The differences between the PSF values obtained with different Fermi functions are also reflected in the electron spectra. To obtain the summed energy spectra of electrons, we changed the integration variables from the individual electrons kinetic energies to their sum

Table 1. Phase space factors computed with Fermi functions in approximation schemes A, B, C. Values are obtained with equations (9), (10). Q-values are also displayed.

Nucleus	Q^{a}(keV)	$G^{2\nu}$ in units of 10^{-21} yr^{-1}		
		A	B	C
^{48}Ca	4268.070 ± 0.076	12051.21 ± 2.02	15941.38 ± 2.66	15212.54 ± 2.54
^{76}Ge	2039.059 ± 0.014	25.755 ± 0.002	52.834 ± 0.003	48.384 ± 0.003
^{82}Se	2997.9 ± 0.3	828.96 ± 0.75	1779.02 ± 1.58	1597.40 ± 1.42
^{100}Mo	3034.40 ± 0.17	1241.83 ± 0.62	3822.34 ± 1.89	3312.62 ± 1.63
^{110}Pd	2017.85 ± 0.64	40.32 ± 0.11	163.07 ± 0.43	138.57 ± 0.37
^{116}Cd	2813.50 ± 0.13	776.81 ± 0.32	3318.62 ± 1.33	2767.61 ± 1.11
^{130}Te	2527.515 ± 0.260	344.24 ± 0.31	1891.38 ± 1.66	1538.53 ± 1.35
^{136}Xe	2458.13 ± 0.41	287.56 ± 0.42	1797.71 ± 2.55	1441.47 ± 2.04
Nucleus	Q^{a}(keV)	$\delta G^{2\nu}/(10 \mathring{a}_{of}^{(3)})$ in units of 10^{-21} yr^{-1} MeV^{-1}		
		A	B	C
^{48}Ca	4268.070 ± 0.076	5318.08 ± 0.81	7002.59 ± 1.06	6674.90 ± 1.01
^{76}Ge	2039.059 ± 0.014	21.754 ± 0.001	44.195 ± 0.002	40.446 ± 0.002
^{82}Se	2997.9 ± 0.3	497.02 ± 0.40	1054.26 ± 0.84	945.27 ± 0.75
^{100}Mo	3034.40 ± 0.17	733.70 ± 0.33	2219.94 ± 0.99	1920.26 ± 0.85
^{110}Pd	2017.85 ± 0.64	34.09 ± 0.08	135.41 ± 0.32	114.94 ± 0.27
^{116}Cd	2813.50 ± 0.13	489.48 ± 0.18	2046.83 ± 0.74	1703.76 ± 0.61
^{130}Te	2527.515 ± 0.260	238.08 ± 0.19	1277.20 ± 1.00	1036.90 ± 0.81
^{136}Xe	2458.13 ± 0.41	203.69 ± 0.27	1241.58 ± 1.57	993.53 ± 1.26

^{a} See appendix for details on Q-values.

$K = \epsilon_1 + \epsilon_2$ and their difference $T = \epsilon_1 - \epsilon_2$ with $K \in [0, Q]$ and $T \in [-K, K]$. In figures 1 and 2 are plotted the energy spectra (upper part) and their deviations due to LIV (lower part) corresponding with equations (4) and (7), respectively. The legends in figures 1 and 2 are related to the approximation schemes for the Fermi functions discussed in section 3. The spectra corresponding to the LIV component are presented independently of the coefficient $\mathring{a}_{of}^{(3)}$.

It can be observed that the use of non-relativistic Fermi functions (A scheme) gives spectra that differ much from those obtained with relativistic Fermi functions (B, C schemes). Also, there are significant differences between the electron spectra obtained with approximations B and C. Hence, the use of accurate Fermi functions is important for obtaining reliable summed energy spectra of electrons. Further, looking to the lower part of the figures, one observes that the standard electron spectra should be shifted if LIV effects are present. To highlight this shift, a vertical line passing through the maximum of the standard spectrum was drawn in the figures. We note that, at request, we can provide experimentalists with the numerical data needed to build up theoretical electron spectra.

6. Quantities of experimental interest

In LIV investigations, an important parameter is also the value of the summed energy of electrons where the LIV effect is expected to be maximum. This energy, K_m, corresponds to the position where the LIV summed energy spectrum of electrons is maximal [9]. This quantity is dependent on all the input ingredients taken into account in spectrum computation
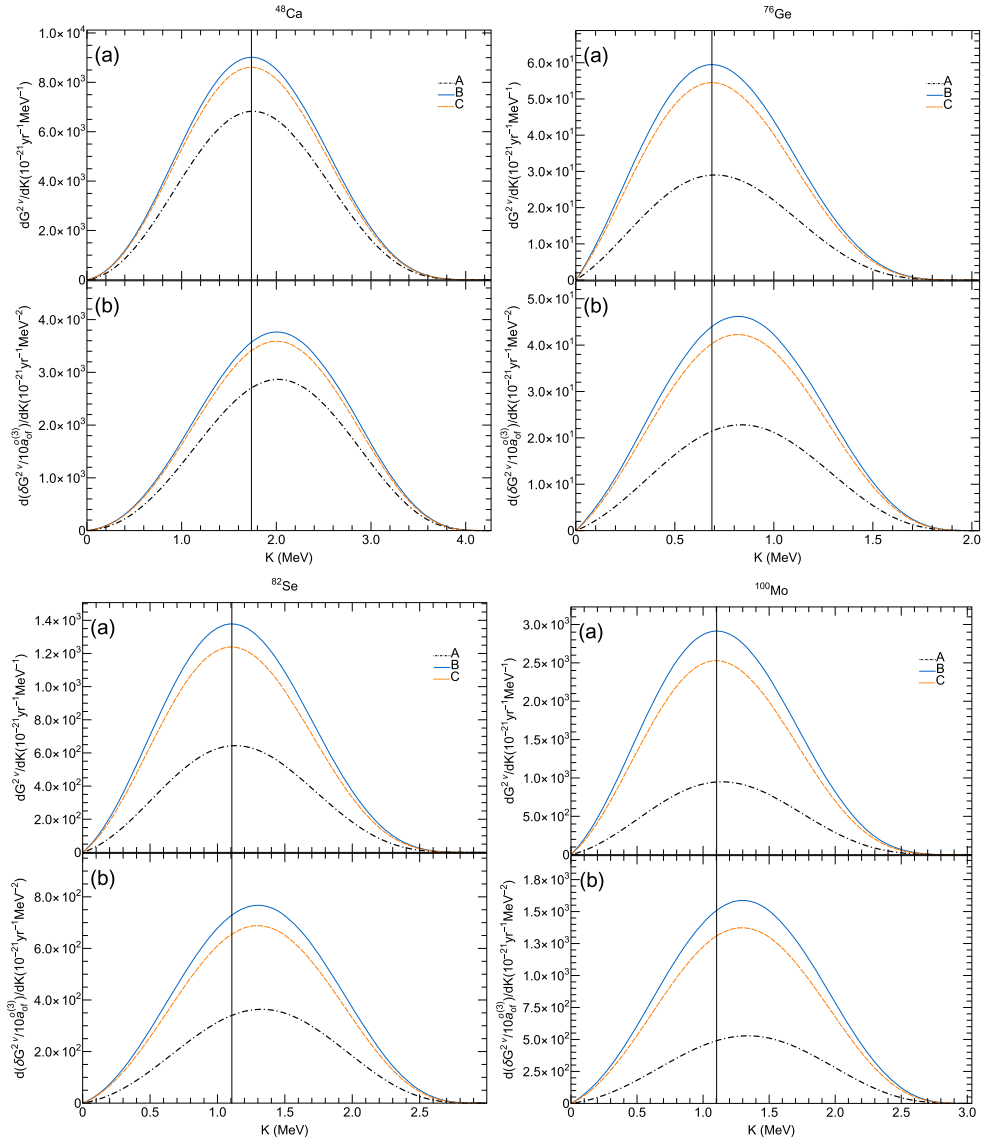
Figure 1. Summed energy spectra of electrons in the standard $2\nu\beta\beta$ decay (a) and their deviations due to LIV (b) for the nuclei ^{48}Ca, ^{76}Ge, ^{82}Se and ^{100}Mo.

(Fermi function, Q-value, the inclusion of kinematic factors). As seen in figures 1 and 2, the deviation should not be large since all spectra have similar shapes. We computed these positions and presented them in table 2 together with the ones reported in [9]. The values in the third column were obtained by employing the full treatment of the $2\nu\beta\beta$ decay rate, namely using numerical Fermi functions obtained with approximation scheme C, taking the Q-values given in the appendix and including the kinematic factors.

The last column of table 2 contains the ratio of the integrals in equations (4) and (7) which is independent of the LIV coefficient $\mathring{a}_{of}^{(3)}$ and that is the needed input for LIV effects (as shown in [20]). The values presented in this column are computed using the same
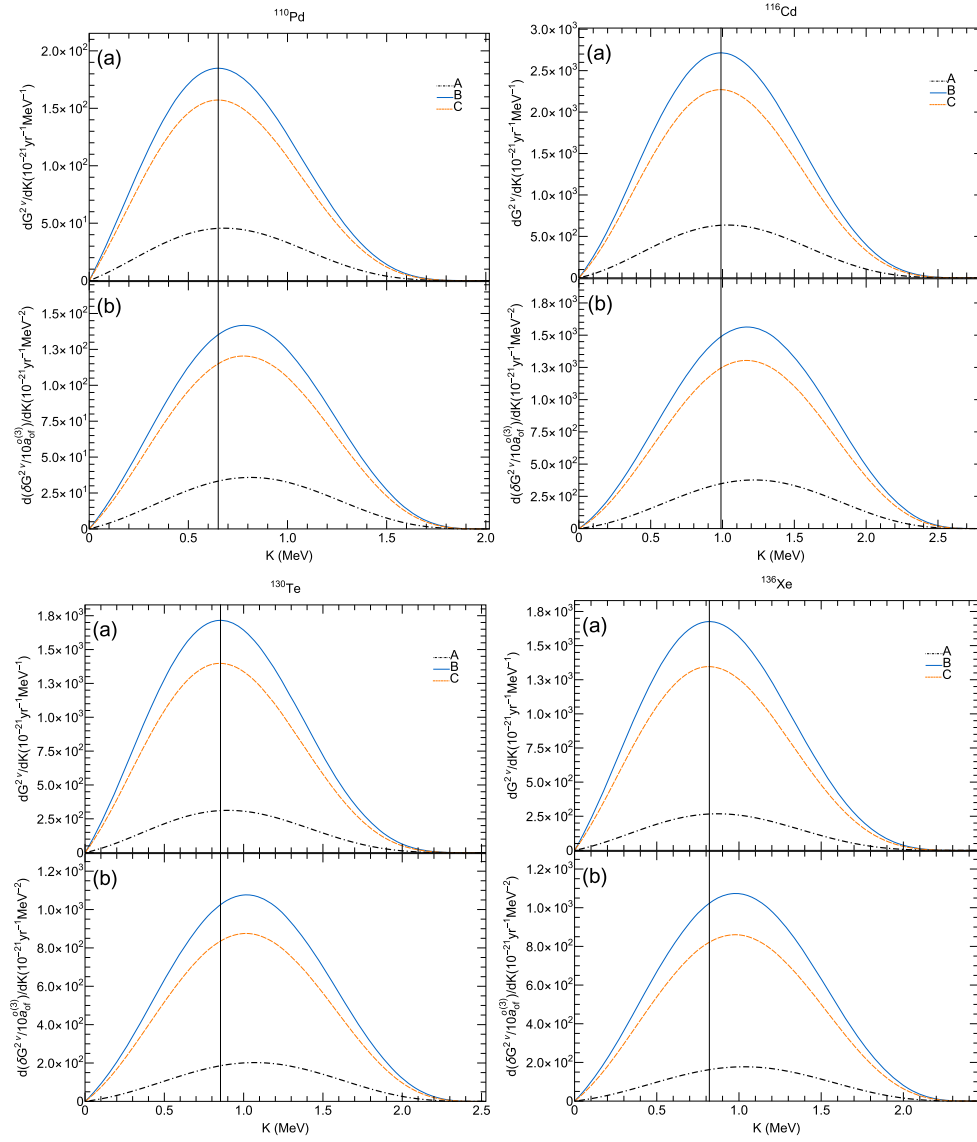
Figure 2. Summed energy spectra of electrons in the standard $2\nu\beta\beta$ decay (a) and their deviations due to LIV (b) for the nuclei ^{110}Pd, ^{116}Cd, ^{130}Te and ^{136}Xe.

treatment as for the ones in the third column. We note the difference between our prediction of the ratio $\mathring{a}_{of}^{(3)}G^{2\nu}/\delta G^{2\nu}$ for ^{82}Se (168.823×10^{-6} GeV) and the one given in [20] (213.3×10^{-6} GeV) to constrain the coefficient $\mathring{a}_{of}^{(3)}$.

7. Conclusions

Investigations of LIV effects are currently also conducted in DBD, particularly by searching for deviations of the summed energy spectra of electrons in $2\nu\beta\beta$ decays from their standard

Table 2. K_m—energy where LIV effect is maximal and $\mathring{a}_{of}^{(3)}G^{2\nu}/\delta G^{2\nu}$—ratio calculated with formulas (4) and (7).

Nucleus	K_m(keV)[9]	K_m(keV)	$\mathring{a}_{of}^{(3)}G^{2\nu}/\delta G^{2\nu}$ (10^{-6}GeV)
^{48}Ca	1980	2002	227.199 ± 0.048
^{76}Ge	810	818	119.562 ± 0.009
^{82}Se	1300	1297	168.823 ± 0.195
^{100}Mo	1320	1294	172.365 ± 0.111
^{110}Pd	⋯	777	120.518 ± 0.420
^{116}Cd	1200	1165	162.339 ± 0.085
^{130}Te	1050	1013	148.307 ± 0.170
^{136}Xe	1020	980	145.023 ± 0.269

forms. In the absence of observing such deviations, constraints are placed on the $\mathring{a}_{of}^{(3)}$ coefficient that controls the strength of the LIV associated with the time-like component of the countershaded operator in SME theory. For the experimental investigations, theoretical calculations of PSF, summed energy spectra of electrons, and their deviations due to LIV are needed. In this work, we provide accurate calculations of these quantities using exact electron wave functions for building the Fermi functions with the inclusion of finite nuclear size and screening effects, Q-values obtained by averaging on values provided by experimental measurements and PSF expressions that include the kinematic factors. Comparing our results with previous ones used in other LIV investigations, we show that the choice of the Fermi functions is the essential ingredient in calculations. We obtained differences up to about 30% even between different relativistic methods of calculation of these functions. We estimate the uncertainties in the computation of these quantities associated with experimental measurements of the Q-values and with the omission of the kinematic factors in the PSF expressions. Uncertainties in the PSF values due to the use of inaccurate Q-values are nucleus-dependent and are estimated at $8 \times \sigma_Q/Q$. Next, we calculated with our method described in section 3.3 and [25, 26] the quantities of experimental interest in LIV analyses, namely the ratios between the standard PSF and their LIV deviations.

Precise calculations can significantly influence the theoretical data needed in LIV analyses. As an example, we found a relevant difference between our obtained value of this ratio and the one used by the CUPID-0 collaboration. Hence, we hope that our theoretical predictions corroborated with a precise analysis of the summed energy spectra of electrons lead to improved constraints on the $\mathring{a}_{of}^{(3)}$ coefficient that controls the LIV strength of the time-like component of the countershaded operator in SME.

Acknowledgments

Appendix

One of the most important parameters in the computation of the PSF is the Q-value of the double-beta decay. In this study, we treated the uncertainty associated with the Q-value as the only source of uncertainty in the PSF. There are multiple experimental values reported in the

Table A1. Experimental Q values and the average Q-values for g.s. to g.s. transitions.

Parent nucleus	Measured energies(keV)		Average value	
			$Q \pm \sigma_Q$(keV)	S
^{48}Ca	4262.96 ± 0.84 [40]	4268.121 ± 0.079 [41]		
	4267.98 ± 0.32 [42]		4268.070 ± 0.076	1.0
^{76}Ge	2038.56 ± 0.32 [43]	2038.58 ± 0.31 [44]		
	2039.006 ± 0.05 [45]	2039.04 ± 0.16 [46]		
	2039.061 ± 0.007[47]		2039.059 ± 0.014	2.0
^{82}Se	2997.9 ± 0.3 [48]		2997.90 ± 0.30	
^{100}Mo	3034.0 ± 6.0 [49]	3034.40 ± 0.17 [46]	3034.40 ± 0.17	1.0
^{110}Pd	2017.85 ± 0.64 [50]		2017.85 ± 0.64	
^{116}Cd	2813.50 ± 0.13 [51]		2813.50 ± 0.13	
^{130}Te	2527.01 ± 0.32 [52]	2527.518 ± 0.013 [53]		
	2526.97 ± 0.23 [51]		2527.51 ± 0.26	2.0
^{136}Xe	2479.0 ± 79.0 [54]	2462.7 ± 4.3 [55]		
	2457.83 ± 0.37 [56]	2458.73 ± 0.56 [57]	2458.13 ± 0.41	1.3

literature for different double-beta decays, and the use of one or another influences the PSF calculated values and predictions of the electron spectra. The choice of the Q-values used in the PSF calculation is made as follows. For each $2\nu\beta\beta$ decay, we collect the Q_i-values from the literature together with their statistical errors (δQ_i). Then, we calculate an average Q-value and the statistical error for each decay following a procedure presented in [27] that we shortly describe here.

A Q-value for a particular DBD is measured in N independent experiments. For the set of measurements obtained, $x_i \pm \delta x_i$, a Gaussian distribution is considered. Here $x_i = Q_i$ and $\delta x_i = \delta Q_i$ are the value and the error provided by the i-experiment, respectively. The weighted average and the corresponding error are calculated with the following equation:

$$\bar{x} \pm \delta\bar{x} = \frac{\sum w_i x_i}{\sum w_i} \pm \left(\sum w_i\right)^{-1/2}, \tag{A.1}$$

where

$$w_i = \frac{1}{(\delta x_i)^2} \tag{A.2}$$

and the sums run over all N experiments. For each weighted average, we calculated $\chi^2 = \sum w_i(\bar{x} - x_i)^2$ and a scale factor, S, defined as

$$S = \left(\frac{\chi^2}{N-1}\right)^{1/2} \tag{A.3}$$

to establish if the measurements are indeed from a Gaussian distribution. If the scale factor is less than or equal to 1, the value of $\delta\bar{x}$ is left unchanged, and the result is accepted. If S is larger than 1 and the inputs δx_i are all about the same size, then we increase $\delta\bar{x}$ by the scale factor. In the final case of S larger than 1 and the δx_i are of widely varying magnitudes, S is recalculated with only the input for which $\delta x_i \leqslant 3N^{1/2}\delta\bar{x}$. In all cases, the original value of $\bar{x}$ remains unchanged.

The results of this procedure are displayed in table A1 where the first column contains the studied nuclei. The second column contains the experimental data available for each nucleus. The average Q-values and their uncertainties (σ_Q) obtained with the procedure described

Table A2. Phase space factors (upper part) and their deviations (lower part) computed with numerical Fermi functions and with inclusion of kinematic factors. Relative uncertainties associated with Q-values are displayed in column 3, in terms of σ_Q/Q. Differences introduced by the omission of kinematic factors: $\xi = (G - G^{\text{No VS}})/G$ and $\delta\xi = (\delta G - \delta G^{\text{No VS}})/\delta G$ are also displayed in the last column ($G^{\text{No VS}}$ and $\delta G^{\text{No VS}}$ are the ones from table 1).

Nucleus	G $(10^{-21}$ yr$^{-1})$	$\sigma_G/G \left(\frac{\sigma_Q}{Q}\right)$	$\xi(\%)$
^{48}Ca	15443.23	8.83	1.494
^{76}Ge	48.50	8.32	0.231
^{82}Se	1604.65	8.58	0.452
^{100}Mo	3325.32	8.53	0.382
^{110}Pd	138.79	8.20	0.158
^{116}Cd	2775.55	8.43	0.286
^{130}Te	1541.74	8.32	0.208
^{136}Xe	1444.19	8.29	0.188
Nucleus	$\delta G/(10\mathring{a}_{0f})(10^{-21}$ yr^{-1} MeV$^{-1})$	$\sigma_{\delta G}/\delta G \left(\frac{\sigma_Q}{Q}\right)$	$\delta\xi(\%)$
^{48}Ca	6797.21	7.94	1.800
^{76}Ge	40.56	7.43	0.284
^{82}Se	950.49	7.69	0.549
^{100}Mo	1929.23	7.64	0.465
^{110}Pd	115.16	7.31	0.195
^{116}Cd	1709.73	7.54	0.349
^{130}Te	1039.56	7.43	0.255
^{136}Xe	995.83	7.39	0.231

above are presented in the third column, while the resulting scaling factor S is shown in the last column.

Since this procedure provides also an averaged uncertainty for each Q-value, an estimation of the uncertainties in the PSF can be easily made as follows. Let f denote both G and δG factors which depend on the Q-value, which is subject to some uncertainty σ_Q. Then, since Q is the only source of error accounted for in this study, the uncertainty in f can be computed using the formula

$$\sigma_f = \left(\frac{\partial f}{\partial Q}\right)\sigma_Q. \tag{A.4}$$

As seen in table A1, the uncertainty in Q is reflected significantly in the PSF uncertainty.

The use of more accurate expressions for the kinematic factors $\langle K_N \rangle$ and $\langle L_N \rangle$ (equations (5) and (6), instead of (8)) also gives differences in the calculations of PSF, summed energy spectra of electrons and their deviations due to LIV, but with smaller effects than in the case of using different Q-values. In table A2 we report the PSF values (upper part) and their deviations (lower part) computed with numerical Fermi functions (approximation C) and inclusion of the kinematic factors.

The third column displays the relative uncertainty in the PSF values in terms of relative uncertainties in the Q-values. As a rule of thumb, the relative uncertainty in the PSF is between 8 and 9 times (Standard) and between 7 and 8 times (LIV) the one of the Q-value. The last column of table A2 contains the differences in percentages between the calculated

values with inclusion or not of the kinematic factors. As seen, there are small deviations associated with this approximation, the largest ones being at ^{48}Ca nucleus.

ORCID iDs

O Nițescu ● https://orcid.org/0000-0002-9598-8415
S Ghinescu ● https://orcid.org/0000-0003-3716-9857
S Stoica ● https://orcid.org/0000-0003-4632-7327

References

[1] Colladay D and Kostelecký V A 1997 *Phys. Rev.* D **55** 6760
[2] Colladay D and Kostelecký V A 1998 *Phys. Rev.* D **58** 116002
[3] Kostelecký V A 2004 *Phys. Rev.* D **69** 105009
[4] Kostelecký V A and Russell N 2011 *Rev. Mod. Phys.* **83** 11–31
[5] Alan Kostelecký V and Mewes M 2004 *Phys. Rev.* D **69** 016005
[6] Adam T *et al* (The OPERA collaboration) 2012 *J. High Energy Phys.* JHEP10(2012)093
[7] Díaz J S, Kostelecký V A and Lehnert R 2013 *Phys. Rev.* D **88** 071902
[8] Díaz J S 2014 *Adv. High Energy Phys.* **2014** 962410
[9] Díaz J S 2014 *Phys. Rev.* D **89** 036002
[10] Abe Y *et al* (Double Chooz Collaboration) 2012 *Phys. Rev.* D **86** 112009
[11] Aguilar-Arevalo A A *et al* (MiniBooNE Collaboration) 2013 *Phys. Lett.* B **718** 1303–8
[12] Abbasi R *et al* (IceCube Collaboration) 2010 *Phys. Rev.* D **82** 112003
[13] Adamson P *et al* (The MINOS Collaboration) 2012 *Phys. Rev.* D **85** 031101
[14] Abe K *et al* (Super-Kamiokande Collaboration) 2015 *Phys. Rev.* D **91** 052003
[15] Albert J B *et al* (EXO-200 Collaboration) 2016 *Phys. Rev.* D **93** 072001
[16] Pertoldi L 2017 Search for Lorentz and CPT symmetries violation in double-beta decay using data from the GERDA experiment *PhD Thesis* Universita degli Studi di Padova
[17] Arnold R *et al* 2019 *Eur. Phys. J.* C **79** 440
[18] Brofferio C, Cremonesi O and Dell'Oro S 2019 *Front. Phys.* **7** 86
[19] Nutini I 2019 The CUORE experiment: detector optimization and modelling and CPT conservation limit *PhD Thesis* INFN—Gran Sasso Science Institute
[20] Azzolini O *et al* 2019 *Phys. Rev.* D **100** 092002
[21] Primakoff H and Rosen S P 1959 *Rep. Prog. Phys.* **22** 121–66
[22] Haxton W and Stephenson G 1984 *Prog. Part. Nucl. Phys.* **12** 409–79
[23] Doi M, Kotani T and Takasugi E 1985 *Prog. Theor. Phys. Suppl.* **83** 1–175
[24] Suhonen J and Civitarese O 1998 *Phys. Rep.* **300** 123–214
[25] Stoica S and Mirea M 2013 *Phys. Rev.* C **88** 037303
[26] Mirea M, Pahomi T and Stoica S 2015 *Rom. Rep. Phys.* **67** 872–89
[27] Olive K A *et al* 2014 *Chin. Phys.* C **38** 090001
[28] Kostelecký V A and Tasson J D 2009 *Phys. Rev. Lett.* **102** 010402
[29] Vergados J D, Ejiri H and Šimkovic F 2012 *Rep. Prog. Phys.* **75** 106301
[30] Konopinski E J 1966 *The Theory of Beta Radioactivity International Series of Monographs on Physics* (Oxford: Clarendon)
[31] Haxton W C, Stephenson G J and Strottman D 1982 *Phys. Rev.* D **25** 2360–9
[32] Rose M E 1961 *Relativistic Electron Theory* (New York: Wiley)
[33] Kotila J and Iachello F 2012 *Phys. Rev.* C **85** 034316
[34] Esposito S 2002 *Am. J. Phys.* **70** 852–6
[35] Salvat F and Mayol R 1991 *Comput. Phys. Commun.* **62** 65–79
[36] Salvat F, Fernández-Varea J and Williamson W 1995 *Comput. Phys. Commun.* **90** 151–68
[37] Salvat F, Fernández-Varea J and Williamson W J 2016 RADIAL: a FORTRAN subroutine package for the solution of the radial Schrodinger and Dirac wave equations http://users.df.uba.ar/dmitnik/estructura3/programas/salvat/radial.pdf
[38] Štefánik D C V, Dvornický R, Šimkovic F and Vogel P 2015 *Phys. Rev.* C **92** 055502
[39] Šimkovic F, Dvornický R, Štefánik D C V and Faessler A 2018 *Phys. Rev.* C **97** 034315

[40] Redshaw M, Bollen G, Brodeur M, Lincoln D L, Bustabad S, Novario S J, Ringle R and Schwarz S 2012 *Phys. Rev.* C **86** 041306
[41] Bustabad S, Bollen G, Brodeur M, Lincoln D L, Novario S J, Redshaw M, Ringle R, Schwarz S and Valverde A A 2013 *Phys. Rev.* C **88** 022501
[42] Kwiatkowski A A *et al* 2014 *Phys. Rev.* C **89** 045502
[43] Hykawy J G, Nxumalo J N, Unger P P, Lander C A, Barber R C, Sharma K S, Peters R D and Duckworth H E 1991 *Phys. Rev. Lett.* **67** 1708–11
[44] Hykawy J, Nxumalo J, Unger P, Lander C, Peters R, Barber R, Sharma K and Duckworth H 1993 *Nucl. Instrum. Methods Phys. Res.* A **329** 423–32
[45] Douysset G, Fritioff T, Carlberg C, Bergström I and Björkhage M 2001 *Phys. Rev. Lett.* **86** 4259–62
[46] Rahaman S *et al* 2008 *Phys. Lett.* B **662** 111–6
[47] Mount B J, Redshaw M and Myers E G 2010 *Phys. Rev.* C **81** 032501
[48] Lincoln D L, Holt J D, Bollen G, Brodeur M, Bustabad S, Engel J, Novario S J, Redshaw M, Ringle R and Schwarz S 2013 *Phys. Rev. Lett.* **110** 012501
[49] Nelson M A 1995 *PhD Thesis* University of California
[50] Fink D *et al* 2012 *Phys. Rev. Lett.* **108** 062502
[51] Rahaman S, Elomaa V V, Eronen T, Hakala J, Jokinen A, Kankainen A, Rissanen J, Suhonen J, Weber C and Yst J 2011 *Phys. Lett.* B **703** 412–6
[52] Scielzo N D *et al* 2009 *Phys. Rev.* C **80** 025501
[53] Redshaw M, Mount B J, Myers E G and Avignone F T 2009 *Phys. Rev. Lett.* **102** 212502
[54] Avignone F T, King G S and Zdesenko Y G 2005 *New J. Phys.* **7** 6–6
[55] Herlert A 2006 *Int. J. Mass Spectrom.* **251** 131–7
[56] Redshaw M, Wingfield E, McDaniel J and Myers E G 2007 *Phys. Rev. Lett.* **98** 053003
[57] McCowan P M and Barber R C 2010 *Phys. Rev.* C **82** 024603